

Structural characterization of double stacking faults induced by cantilever bending in nitrogen-doped 4H-SiC

G. REGULA*†, M. LANCIN†, H. IDRISSE†,
B. PICHAUD† and J. DOUIN‡§

†Thermodynamique, Propriétés Electriques, Contraintes et Structures anx
Echelles Nanométriques, Unité Mixte de Recherche associée au CNRS 6122,
Université Paul Cézanne, 13397 Marseille Cedex 20, France

‡Laboratoire d'Etudes des Microstructures, Laboratoire Mixte ONERA–CNRS,
BP 72, 92332 Châtillon Cedex, France

(Received 17 February 2005; in final form 14 March 2005)

Defects in highly nitrogen-doped 4H-SiC deformed by cantilever bending at 550°C have been identified by weak-beam and high-resolution transmission electron microscopy techniques. The induced-defects consist of double stacking faults (DSFs) whose expansion produces a local 4H → 3C phase transformation. Each DSF is bound by two identical 30° Si(g) partial dislocations which glide on two adjacent basal planes. The DSFs belong to three different populations which differ by their extension as a function of the applied-stress and the 30° Si(g) characteristics (line direction L , Burgers vector b , glide planes and glide direction). The external mechanical stresses are the main driving forces involved in the DSF expansion. However, extra driving forces such as thermodynamic or electronic forces are also likely to be involved.

1. Introduction

As 4H-SiC is both a wide-band gap semiconductor and a structural ceramic, it holds promise for operations at high power levels and in harsh environments. However, despite the high crystalline perfection of the wafers now available, the use of SiC still remains restricted because of the expansion of device-killer stacking faults (SFs) dragged by Shockley partial dislocations under forward biasing of bipolar devices [1–11]. In addition, the formation of double stacking faults (DSFs) bound by two Shockley partial dislocations during oxidation [12], annealing [13–15] or high-temperature processing [16] of highly nitrogen-doped 4H-SiC (10^{18} – 10^{19} cm⁻³) has also been reported. The nucleation and formation of these defects are still a matter of concern and thus receive considerable attention from the viewpoint of both applied

*Corresponding author. Email: gabrielle.regula@univ.u-3mrs.fr

§Present address: Centre d'Elaboration des Matériaux et d' Etudes Structurales, Unité Propre de Recherche associée an CNRS 8011, 29 rue Jeanne Marvig, BP 94347, 31055 Toulouse Cedex 4, France.

and fundamental science. The discussion of the data is based on parameters that control the dislocation nucleation and expansion. They are obtained either from theoretical calculations [17–19] or from plasticity experiments (indentation or constant-displacement compression tests) performed in highly nitrogen-doped 4H-SiC, from room temperature up to 1400°C [20–24]. Until now, discrepancies still exist between theoretical and experimental results. As an example it was experimentally shown that Shockley partial dislocations with a silicon core (Si(g)) have a significantly lower nucleation barrier than those with a carbon core (C(g)) and that Si(g) is more mobile than C(g) while, on the contrary, according to calculations, C(g) should exhibit a higher thermal mobility than Si(g).

In order to contribute to the debate, we have developed a procedure to measure directly the dynamic parameters of dislocations in 4H-SiC. We have selected materials with a doping level similar to those used in previous plasticity studies reported in the literature. This letter deals with the characterization of the defects involved in these measurements using optical microscopy, weak-beam (WB) transmission electron microscopy (TEM) and high-resolution transmission electron microscopy (HRTEM) techniques.

2. Materials and techniques

The samples were cut from nitrogen-doped ($5 \times 10^{18} \text{ cm}^{-3}$) 4H-SiC wafers purchased from CREE Research. In order to optimize the deformation procedure, we selected wafers with a $(11\bar{2}0)$ surface orientation and cut the $(20 \text{ mm} \times 5 \text{ mm} \times 0.25 \text{ mm})$ samples so that the glide planes were at 45° from the tension/compression axis X (figure 1). Dislocation sources were created by a scratch parallel to X on the sample surface. The samples were then bent at room temperature around the Y direction, resulting in dislocation sources under compressive stress the intensity of which varies linearly along the X direction. Note that a complex local stress (whose intensity is not linearly X dependent) produced by the scratch procedure itself would have tensile components. Finally, the samples were annealed under stress at 550°C for 30 min. The $(11\bar{2}0)$ surfaces of the deformed-samples were observed with a Reichert optical microscope after etching with molten KOH (500°C for 10 min). WB images were performed with a JEOL 200CX on (0001) thin foils prepared by

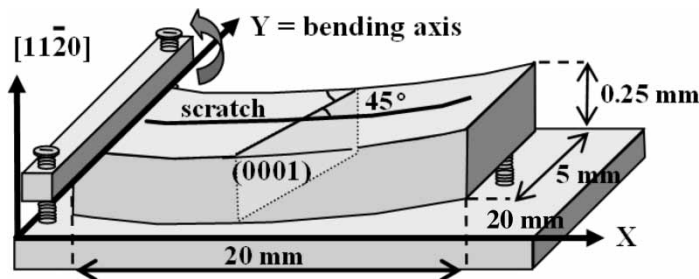


Figure 1. Schematic diagram of the cantilever bending set-up.

the focused-ion-beam (FIB) technique in order to observe the dislocations near the sample surface. HRTEM studies were carried out with a JEOL 2010-FEG on $(11\bar{2}0)$ thin foils prepared by back-side mechanical polishing and ion-beam milling. Samples were imaged at the minimum of contrast (white atoms) or at the Scherzer defocus (black atoms). The image contrast simulation was performed using the multislice method (EMS software [25]).

3. Results

The images displayed in figure 2 are typical of samples chemically etched after deformation. Dark straight lines (instead of dots) parallel to the basal plane are revealed in figure 2a. They are fingerprints of SF intersections with the sample surface. These SFs will be labelled SFAs hereafter. SFAs are nucleated from the scratch but also from one of the sample edges damaged by the cutting. They propagate solely in the P1 direction under the applied stress σ . Their length increases versus σ from about zero to the sample half-width. Another population of stacking faults, labelled SFBs, expands from the scratch or from the sample edge in the P1 direction. These SFBs are difficult to detect among the SFAs by optical microscopy even at a high magnification (figure 2b) but they were clearly identified by TEM techniques. Their length remains smaller than about $200\ \mu\text{m}$. A third population of SFs, labelled SFCs, is also revealed in figure 2b. These SFCs expand in the P2 direction solely from the scratch and their length decreases from about $400\ \mu\text{m}$ to zero when σ increases. Note that individual etch pits characteristic of emerging perfect or dissociated dislocations were never observed.

The WB micrographs obtained at the tip of ten SFA, five SFB and three SFC etched lines always reveal not one but two SFs dragged by a pair of Shockley partial dislocations. For the SFAs, both partial dislocations D1 and D2 are always perfectly aligned along $[\bar{1}2\bar{1}0]$ Peierls valleys (figure 3a). Using the extinction criterion, we obtained for both partial dislocations the same Burgers vector $\mathbf{b} = \pm(a/3)[\bar{1}100]$. As \mathbf{b} makes a 30° angle with the lines, the partial dislocations have a 30° character. Concerning the SFBs, D1 and D2 partial dislocations are almost parallel to $[11\bar{2}0]$

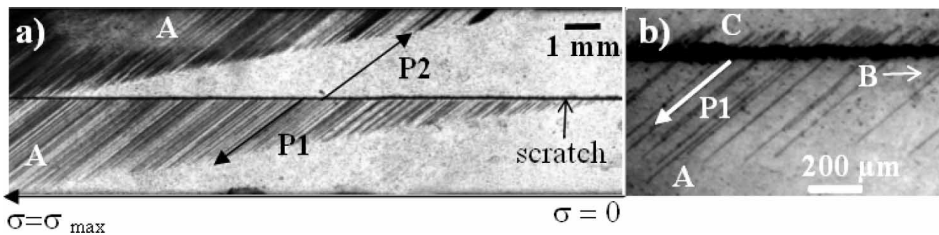


Figure 2. Optical micrographs of the $(11\bar{2}0)$ sample surface after cantilever bending at 550°C for 30 minutes and chemical etching. (a) The $\{0001\}$ planes are at 45° from the scratch, which lays along the tension compression axis X . The etched lines reveal the intersections of stacking faults A with the sample surface. (b) Zoom of the etching pattern close to the scratch showing the A, B and C populations of stacking faults which expand in the P1 direction ($[1100]$) or the P2 direction ($[11\bar{2}0]$).

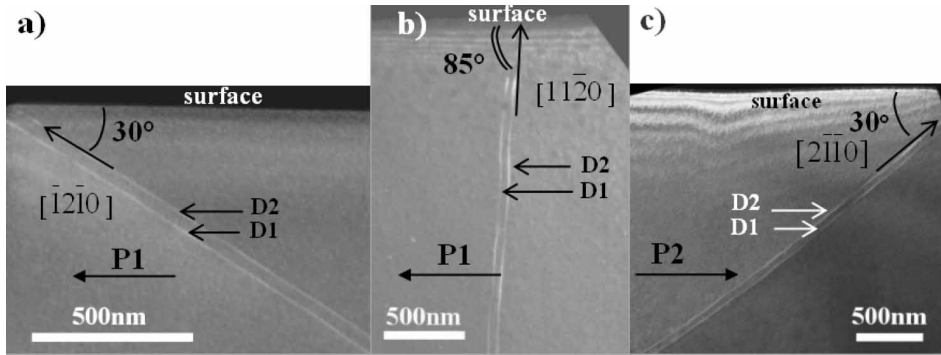


Figure 3. WB TEM images of the dislocations obtained near their emergency at the $(11\bar{2}0)$ sample surface. They were taken near the $[0001]$ zone axis with (a) $g = 1210$ for SFA (b) $g = 1120$ for SFB and (c) $g = 2\bar{1}10$ for SFC. P1 and P2 indicate the directions of dislocation propagation. Owing to the chosen diffraction conditions, the SFs are out of contrast.

Peierls valleys (figure 3b). We found $\mathbf{b} = \pm(a/3)[01\bar{1}0]$ for both D1 and D2, showing that they are also 30° partial dislocations. D1 and D2 partial dislocations observed in the SFCs exhibit a slightly curved line (figure 3c). At the emerging point, the lines are nearly parallel to $[2\bar{1}\bar{1}0]$ Peierls valleys. As their Burgers vector is $\mathbf{b} = \pm(a/3)[\bar{1}100]$, both partial dislocations have also a 30° character close to the sample surface.

The distance between the glide planes of D1 and D2 was deduced from $(11\bar{2}0)$ HRTEM images of the three SF populations. We have imaged 19 SFAs; 16 SFBs and four SFCs. Figure 4 displays typical $(11\bar{2}0)$ images of SFAs and SFBs, SFCs exhibiting the same stacking as SFBs are not shown. In one $(11\bar{2}0)$ image taken at the minimum of contrast (on the Scherzer defocus respectively), each white (or black respectively) dot corresponds to one Si=C dumbbell formed by the projections of silicon and carbon atomic columns which are 0.109 nm apart (nearest projections). The white or black dots thus reveal the projections of the glide planes belonging to the glide set. The Shockley partial dislocations may glide in the planes labelled G1, G2, G3 or G4 in figure 4. To determine the projections of the silicon and carbon atomic columns within the dots, we first localize the G1–G2 and G3–G4 pair of planes using the ‘black-and-white’ contrast of SiC $(11\bar{2}0)$ images [26]. Then, we use the asymmetry of the dot locations with respect to the $\{0001\}$ projections when the dumbbell orientation changes [27–28]. In figure 4, the atomic structures that we obtained are superimposed on both experimental images (right) and simulated images using these structures (left). Obviously, the SFAs and the SFBs (or SFCs) consist of six cubic layers; however, two symmetrical cubic stackings are observed. The stacking labelled a-3C of the SFAs is the $(\bar{1}100)$ mirror of the stacking labelled b-3C of the SFBs and of the SFCs. Looking at the orientation of the Si=C dumbbells, it is clear that, in order to create the cubic lamellae in between 4H stackings, the shear due to D1 and D2 must occur in adjacent G1 and G2 glide planes to obtain one SFA, and in G3 and G4 glide planes to form one SFB or one SFC. So far, in our experiments, the shear was always produced by the glide of 30° partial dislocations. It is of prime importance to note that the three populations of defects consist

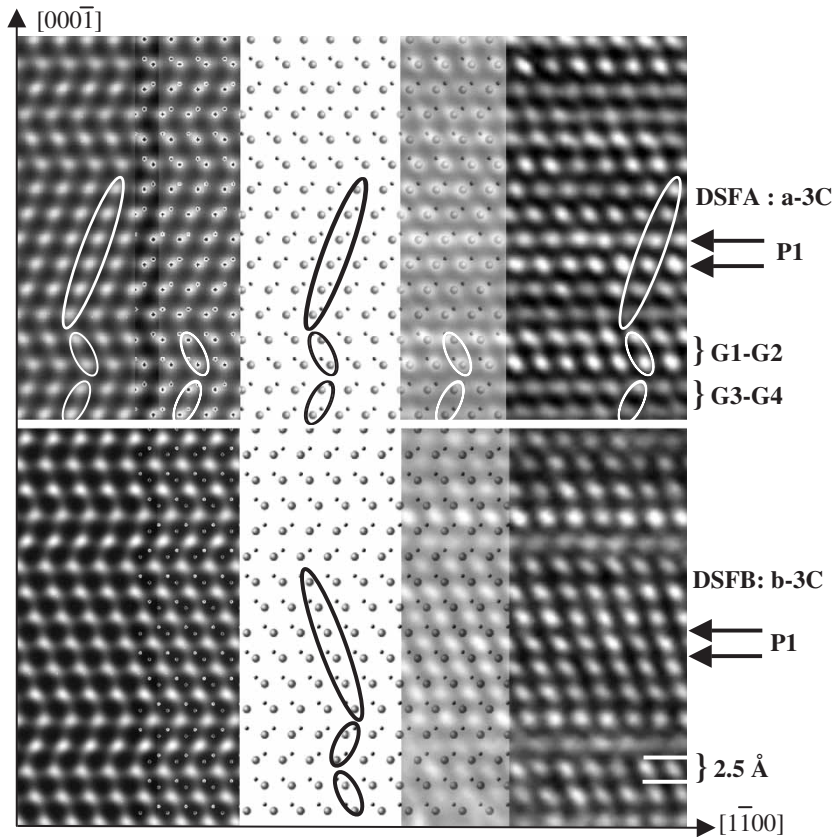


Figure 4. Atomic structures of DSFA and DSFB viewed along the $[1\bar{1}\bar{2}0]$ direction. HRTEM experimental images (right) were taken so that atoms are white (DSFA) or black (DSFB). The atomic structures (middle) deduced from the experimental images are superimposed on them, the large and small dots showing the projections of silicon and carbon atomic columns respectively; on the simulated images (left), the projections of silicon and carbon atomic columns are superimposed by the software; the a-3C stacking and the b-3C stacking are due to the dislocation glide in the G1–G2 and G3–G4 planes respectively (small ellipses show the two types of glide plane and larger ellipses show the 3C stackings). The arrows indicate the glide direction.

actually of DSFs that we shall now label DSFAs, DSFBs and DSFCs. Each of these is dragged by a pair of identical 30° partial dislocations (same line and same \mathbf{b}) gliding on two adjacent slip planes.

The core composition of the partial dislocations was derived from a core reconstruction. The structure of the 4H-SiC and of the crystal sheared by one and by two partial dislocations was projected in the plane perpendicular to the dislocation lines (figure 5). Note that the DSFA and DSFC projections in the $(\bar{1}\bar{2}\bar{1}0)$ and $(2\bar{1}\bar{1}0)$ planes respectively are $(\bar{1}\bar{1}00)$ mirror images of their projections in the $(1\bar{1}\bar{2}0)$ plane (corresponding to figure 4) using to the $P6_3mc$ structure of 4H-SiC. They are thus identical with those of DSFB in the $(1\bar{1}\bar{2}0)$ plane. The propagation direction of the DSFA and DSFB being the same (P1), a unique reconstruction (figure 5a) will

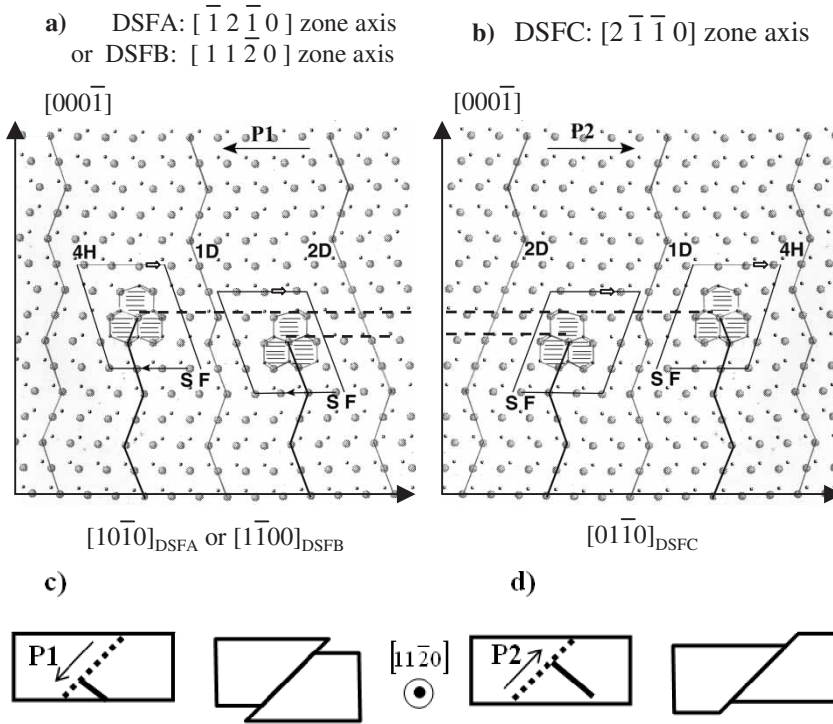


Figure 5. Projection of the dislocation cores in the planes perpendicular to the lines of the 30° partial dislocation bounding (a) the DSFA and DSFB and (b) DSFC and (c), (d) the corresponding sample deformation modes. The upper schemes represent the 4H–1D and 1D–2D reconstructed boundaries where 1D and 2D refer to layers sheared by one or two partial dislocations respectively; the silicon and carbon atomic column projections are shown as large and small dots respectively; the three shaded faulted cycles which are linked by a column of Silicon atoms are characteristic of a 30° Si(g); the projection of glide planes and of the extra half-planes are drawn as dotted lines and bold lines respectively. The closed Burgers circuits were drawn in the perfect crystal following the SF/RH rule. The lower schemes represent a projection in the $(11\bar{2}0)$ plane of extra half-planes and glide planes of DSFAs or DSFBs and of DSFCs and the resulting sample deformation.

provide the dislocation core. Indeed, knowing the propagation direction, P1 or P2, the boundaries are rebuilt in order to obtain the structural unit characteristic of a 30° partial dislocation [28–30]. For the three populations of faults, the reconstruction demonstrates that the core of both partial dislocations consists of a column of silicon atoms and, thus, that the partial dislocations are all of 30° Si(g) type.

The Burgers vectors and line directions of the 30° Si(g) dragging the DSFs were obtained using the WB characterization and the Burgers circuit (Figure 5 (a) and (b)) drawn following the SF/RH rule and with the closed circuit realized in the perfect crystal [31]. We obtained the following for the line orientation L and the Burgers vector b of the dislocations: $L = [1\bar{2}10]$ and $b = (a/3)[1\bar{1}00]$ for the DSFAs, $L = [\bar{1}1\bar{2}0]$ and $b = (a/3)[0\bar{1}10]$ for the DSFBs and $L = [\bar{2}110]$ and $b = (a/3)[1\bar{1}00]$ for the DSFCs.

The reconstructions of the dislocation cores provide the positions of the extra half-planes. Knowing the glide direction of the DSFs it is thus possible to determine

the deformation mode produced by their expansion. As for the DSFAs and the DSFBs, with the extra half-plane pointing downwards from the core, the dislocation glide in the P1 direction induces a compressive strain (figure 5c). On the contrary, the expansion of the DSFCs in the P2 direction results in a tensile strain (figure 5d).

4. Discussion

Three populations of DSFs have been created by our deformation procedure. We recall that the dislocation sources are under compression because of the bending conditions and, thus, that only DSFs releasing a compressive stress can expand as a function of the applied stress σ . This is the case for DSFA and DSFB. Indeed, the DSFA extends over long distances as a function of σ . The very limited extension of DSFBs is probably due to some blocking event. The origin of the DSFC would probably derive from the occurrence of a complex stress field close to the scratch. The development of DSFCs that would release a tensile stress is, however, compatible with the bending conditions, since their length decreases with increasing applied compressive stress. All these points and the origin of the asymmetric expansion of the dislocation loops dragging the DSFs will be discussed further in the light of the new experiments being developed.

The partial dislocations that drag the DSFs are all of the 30° Si(g) type. Their complementary C(g) was never detected at the tip of the DSFs, indicating that partial dislocations with a C core are either immobile or not created. Moreover, no 90° Si(g) dislocations were ever observed as well. All these results are in good agreement with those obtained during deformation experiments by Pirouz and co-workers [20–22, 32]. Indeed, in the same temperature range, when these workers observed single leading partial dislocations without the corresponding trailing partial dislocations, the leading partial dislocations always had a silicon core. They also suggested that, as the 90° Si(g) partial dislocations are more mobile than 30° Si(g), the 90° Si(g) can rapidly leave the samples and cannot be observed.

During their indentation or constant-displacement compression tests, Pirouz and co-workers [20–22, 32] reported the formation of arrays of single SFs or of multiple SFs but never of DSFs. The formation of DSFs cannot be explained by the mechanism proposed by Pirouz *et al.* [33] for the multiple SFs. Indeed, if the resolved shear stress on the cross-slip plane was sufficient to allow the dislocation to cross-slip, it is difficult to understand why only one cross-slip would systematically occur and why multiple cross-slips would not increase with the stress. The formation of DSFs and the surprisingly high dislocation velocity ($v \approx 10^{-6} \text{ m s}^{-1}$ [34]) compared with silicon [35] suggest that driving forces other than mechanical stresses have to be considered. Let us first discuss why DSFs are created. Iwata *et al.* [23, 24] have calculated the formation energy E_{f1} of the first stacking fault and the formation energy E_{f2} of the second SF, leading to the creation of a DSF. They have found that $E_{f2} = 4.7 \text{ mJ m}^{-2}$, which is significantly lower than $E_{f1} = 17.7 \text{ mJ m}^{-2}$. A negative SF energy E_{f2} is even likely because it is well known that the 3C structure is more stable than the 4H structure in that temperature range, particularly for nitrogen-doped SiC [36–38]. Therefore, when a partial dislocation is created to release the applied stress, the formation of a second partial dislocation in the adjacent plane suitable for

creating a DSF is favoured. Once one DSF has been created, the glide of the partial dislocation pairs forms a 3C layer and thus the $4H \rightarrow 3C$ phase transformation is a good candidate as an extra driving force responsible for the high dislocation mobility. Another potential driving force favouring the partial pair mobility and therefore the DSF expansion is the so-called quantum-well action (QWA) [15, 18]. In fact, at 550°C , the Fermi level in our nitrogen-doped SiC is above the lowest energy level associated with the DSF (0.6 eV below the conduction band) [12, 23, 24, 39]. The gain in energy due to the transfer of electrons from the Fermi level to the DSF state helps the extension of the DSF and thus of the associated quantum well. Note that the QWA model is independent of the partial dislocation core and can be considered in experiments where DSFs exist, whether exclusively dragged by Si(g) such as in ours, or by Si(g) and C(g) such as in the work of Chung *et al.* [15]. We emphasize that, according to the above-mentioned reasons, we expect the creation and rapid expansion of DSFs and not of single SFs in the materials deformed by Pirouz and Yang [20]. This discrepancy could originate from differences in the dislocation nucleation modes, nucleation at the surface in our case, and from bulk sources in the case studied by Pirouz and Yang. We are performing complementary studies to clarify better the formation of DSFs.

5. Conclusions

DSFs mechanically introduced in 4H-SiC by cantilever bending result from the glide of pairs of identical 30° Si(g) partial dislocations in adjacent basal planes. No glide of partial dislocations with a carbon core was ever observed. These results are in good agreement with the literature. The DSFs were categorized in three different populations depending on their extension under the applied mechanical stresses. The deformation mode and thus the DSF expansion are determined by the characteristics of the bounding 30° Si(g) pairs, that is their \mathbf{b} , their line direction, their glide planes and their glide direction. The DSFs formation is mainly governed by the external mechanical stresses. However, the formation of DSFs instead of SFs or multiple SFs as reported in the literature indicates that other forces contribute to the deformation mechanism. The $4H \rightarrow 3C$ local phase transformation resulting from the glide of the pairs of partial dislocations and the QWA are good candidates as extra driving forces.

Acknowledgements

The present authors gratefully thank the team of the Centre Pluridisciplinaire et de Microscopie Electronique et de Microanalyse, Université Paul Cézanne, where both FIB experiments and HRTEM observations were performed and ONERA, Châtillon, for the use of conventional JEOL 200CX for WB studies.

References

- [1] H. Lendenmann, F. Dahlquist, N. Johansson, R. Soderholm, P.A. Nilsson, J.P. Bergman and P. Skytt, *Mater. Sci. Forum* **353–356** 727 (2001).

- [2] J.P. Bergman, H. Lendenmann, P.A. Nilsson, U. Lindefelt and P. Skytt, *Mater. Sci. Forum* **353–356** 299 (2001).
- [3] J.Q. Liu, M. Skowronski, C. Hallin, R. Soderholm and H. Lendenmann, *Appl. Phys. Lett* **80** 749 (2002).
- [4] P.O.A. Persson, L. Hultman, H. Jacobson, J.P. Bergman, E. Janzen, J.M. Molina-Aldareguia, W.J. Clegg and T. Tuomi, *Appl. Phys. Lett.* **80** 4852 (2002).
- [5] A. Galeckas, J. Linnros and P. Pirouz, *Appl. Phys. Lett.* **81** 883 (2002).
- [6] M. Skowronski, J.Q. Liu, W.M. Vetter, M. Dudley, C. Hallin and H. Lendenmann, *J. Appl. Phys.* **92** 4699 (2002).
- [7] M.E. Twigg, R.E. Stahlbush, M. Faterni, S.D. Arthur, J.B. Fedison, J.B. Tucker and S. Wang, *Appl. Phys. Lett.* **82** 2410 (2003).
- [8] R.E. Stahlbush, M.E. Twigg, J.J. Sumakeris, K.G. Irvine and P.A. Losee, *Mater. Res. Soc. Symp. Proc.* **815** 103 (2004).
- [9] M. Zhang, P. Pirouz and H. Lendenmann, *Appl. Phys. Lett.* **83** 3320 (2003).
- [10] S. Ha, M. Skowronski, J.J. Sumakeris, M.J. Paisley and M.K. Das, *Phys. Rev. Lett.* **92** 175–504 (2004).
- [11] S. Ha, M. Skowronski and H. Lendenmann, *J. Appl. Phys.* **96** 393 (2004).
- [12] R.S. Okojie, M. Xhang, P. Pirouz, S. Tumakha, G. Jessen and L.J. Brillson, *Appl. Phys. Lett.* **79** 3056 (2001).
- [13] J.Q. Liu, H.J. Chung, T.A. Kuhr, Q. Li and M. Skowronski, *Appl. Phys. Lett.* **80** 2111 (2002).
- [14] T.A. Kuhr, J.Q. Liu, H.J. Chung, M. Skowronski and F. Szmulowicz, *J. Appl. Phys.* **92** 5863 (2002).
- [15] H.J. Chung, J.Q. Liu and M. Skowronski, *Appl. Phys. Lett.* **81** 3759 (2002).
- [16] M. Zhang, H.M. Hobgood, M. Treu and P. Pirouz, *Mater. Sci. Forum* **457–460** 759 (2003).
- [17] P. Sitch, R. Jones, S. Öberg and M.I. Heggie, *Phys. Rev. B* **52** 4951 (1995).
- [18] M.S. Miao, S. Limpijumnong and R.L. Lambrecht, *Appl. Phys. Lett.* **79** 4360 (2001).
- [19] A.T. Blumenu, R. Jones, S. Öberg, P.R. Briddon and T. Frauenheim, *Physica B* **340–342** 160 (2003).
- [20] P. Pirouz and J.W. Yang, *Ultramicroscopy* **51** 189 (1993).
- [21] X.J. Ning, N. Huvey and P. Pirouz, *J. Am. Ceram. Soc.* **80** 1645 (1997).
- [22] A.V. Samant, M.H. Hong and P. Pirouz, *Phys. Stat. Sol. (b)* **222** 75 (2000).
- [23] H.P. Iwata, U. Lindefelt, S. Oberg and P.R. Briddon, *J. Appl. Phys.* **93** 1577 (2003).
- [24] H.P. Iwata, U. Lindefelt, S. Oberg and P.R. Briddon, *J. Appl. Phys.* **94** 4972 (2003).
- [25] P. Stadelman, *Ultramicroscopy* **21** 131 (1987).
- [26] U. Kaiser, A. Chuvilin and W. Richter, *Ultramicroscopy* **76** 21 (1999).
- [27] C. Ragaru, M. Lancin and C. Godon, *J. Eur. Phys.: J. Appl. Phys.* **5** 135 (1999).
- [28] M. Lancin, C. Ragaru and C. Godon, *Phil. Mag. B* **81** 1633 (2001).
- [29] S. Marklung, *Phys. Stat. Sol. (b)* **92** 83 (1979).
- [30] A. Bourret, J. Thibault-Desseaux and F. Lançon, *J. Physique* **9** c4–17 (1983).
- [31] J.P. Hirth and J. Lothe, *Theory of Dislocations* (Wiley, New York, 1982), p. 23.
- [32] P. Pirouz, J.L. Demenet and M.H. Hong, *Phil. Mag A* **81** 1207 (2001).
- [33] P. Pirouz, J.W. Yang, J.A. Powell and F. Ernst, *Inst. Phys. Ser.* 117 (1991).
- [34] H. Idrissi, G. Regula, M. Lancin, J. Douin and B. Pichaud, *Phys. Stat. Sol. (in press)* (2005).
- [35] A. George, Thèse d'Etat, Nancy, France (1977).
- [36] W.F. Knippenberg, *Philips Res. Rep.* **18** 161 238–243 (1963).
- [37] K.L. More, J. Ryu, C.H. Carter, J. Bentley and R.F. Davis, *Adv. in Ceram.* **23** 477 (1987).
- [38] N.W. Jepps and T.F. Page, *J. Am. Ceram. Soc.* **80** C-177 (1981).
- [39] B.J. Skromme, K. Palle, C.D. Poweleit, L.R. Bryant, W.H. Vetter, M. Dudley, K. Moore and T. Gehoski, *Mater. Sci. Forum* **389–393**, 533 (2002).